Proc. NIPR Symp. Upper Atmos. Phys., **6**, 90–102, 1993

SCALE-LENGTH DEPENDENCE OF THE RATIO BETWEEN THE MAGNETIC AND ELECTRIC FIELD PERTURBATIONS IN THE IONOSPHERIC FLELD-ALIGNED CURRENT REGION

Mamoru ISHII[1], Masahisa SUGIURA[2], Toshihiko IYEMORI[3] and James A. SLAVIN[4]

[1] *Department of Geophysics, Faculty of Science, Kyoto University, Sakyo-ku, Kyoto 606*
[2] *Institute of Research and Development, Tokai University, Tomigaya, Shibuya-ku, Tokyo 151*
[3] *Data Analysis Center for Geomagnetism and Space Magnetism, Faculty of Science, Kyoto University, Sakyo-ku, Kyoto 606*
[4] *Goddard Space Flight Center, Greenbelt, Maryland 20771, U.S.A.*

Abstract: There is generally high correlation between the orthogonal magnetic and electric field perturbations on the ionospheric field-aligned current region based on observations by polar orbiting satellites. The ratio between the magnetic and electric field perturbations, $\Delta B_z/\mu_0 E_x$, has a scale-length dependence: the ratio $\Delta B_z/\mu_0 E_x$ decreases with decreasing scale length. B. FORGET *et al.* (J. Geophys. Res., **96**, 1843, 1991) explained this scale-length dependence using a static model. In this paper, we compare the ratio $\Delta B_z/\mu_0 E_x$ observed by the DE-2 satellite for various spatial scales with the effective Pedersen conductivity $\Sigma_{P,eff}$ calculated by the method of FORGET *et al.* The results show that in many cases this model can adequately explain the observed scale-length dependence. However, cases exist in which the difference, $\Delta B_z/\mu_0 E_x - \Sigma_{P,eff}$, decreases at about 0.25–1.0 s in temporal scales (2–8 km in spatial scales). This behavior is explained as being due to Alfvén waves.

1. Introduction

Small scale magnetic and electric field perturbations have been observed in the field-aligned current region in the ionosphere by polar-orbiting satellites. The following results have been obtained from the observations (Table 1): (1) Correlation between the magnetic and electric field perturbations observed in the ionospheric field-aligned current region, especially on the dayside, is often very high. (2) The ratio between the magnetic and electric field perturbations has a scale-length dependence. The ratio $\Delta B_z/E_x$ decreases with decreasing temporal or spatial scale length. There are two interpretations regarding the reason for the correlation between the magnetic and electric field perturbations. One uses a static model; the observed pertubations are regarded as being static spatial variations, and the ratio of the orthogonal magnetic and electric field components, $\Delta B_z/E_x$ represents the height-integrated Pedersen conductivity, Σ_P. The other uses an Alfvén wave model; the observed perturbations are interpreted as being Doppler-shifted Alfvén waves, and the inverse of the ratio gives the Alfvén wave velocity, V_A. The observed perturbations in the magnetic and electric fields may represent a complex mixture of these effects.

Table 1. Investigations on the ratio of the magnetic to electric field perturbation in the high-latitude field-aligned current regions.

Spacecraft	Authors	
ICB-1300	ISRAELEVICH *et al.*	(1988)
	DUBININ *et al.*	(1990)
HILAT and rocket	KNUDSEN *et al.*	(1990)
EXOS-D	MATSUOKA *et al.*	(1991)
AUREOL-3	BERTHELIER *et al.*	(1989)
	FORGET *et al.*	(1991)
Dynamics Explorer 1/2	SUGIURA	(1984)
	SUGIURA *et al.*	(1982, 1983)
	GURNETT *et al.*	(1984)
	WEIMER *et al.*	(1985, 1987)
	ISHII *et al.*	(1992)

FORGET *et al.* (1991) interpreted the scale-length dependence of the ratio between the magnetic and electric field perturbations as being produced by the circumstance that the manner in which a field-aligned current closes its circuit in the ionosphere depends on its scale length. However, they also suggest a possibility of the presence of Alfvén waves. They calculate the scale-length dependence of the height-integrated effective Pedersen conductivity, $\Sigma_{P,\mathrm{eff}}$, solving the current continuity equation numerically.

In this paper, we compare the value of $\Sigma_{P,\mathrm{eff}}$ calculated by the model of FORGET *et al.* with the value of the ratio $\Delta B_z/\mu_0 E_x$ deduced from DE-2 observations. We examine to what extent the Alfvén wave effect exists in scale-length dependence of the ratio $\Delta B_z/E_x$ by subtracting the value of $\Sigma_{P,\mathrm{eff}}$ from the ratio $\Delta B_z/\mu_0 E_x$ calculated from observation.

2. Method of Analysis

We compare the ratio between the magnetic and electric field perturbations deduced from the model, which is the same as that used by FORGET *et al.* (1991), with the ratio based on the observations by DE-2 for 20 examples.

2.1. *Model of FORGET et al.*

The Fourier transformed electrostatic potential, Φ_k, with wave number k in the ionosphere satisfies the following equation (eq. (5) in FORGET *et al.*, 1991):

$$\frac{\mathrm{d}^2\Phi_k}{\mathrm{d}z^2}+\frac{\mathrm{d}\ln\sigma_D}{\mathrm{d}z}\frac{\mathrm{d}\Phi_k}{\mathrm{d}z}-k^2\frac{\sigma_P}{\sigma_D}\Phi_k=0, \tag{1}$$

where σ_D and σ_P represent the direct and Pedersen conductivities, respectively. The z axis is vertical and direct current exists parallel to the $y\cdot z$ plane forming sheet currents. The ambient magnetic field is assumed to be vertical.

We solve this equation for Φ_k for a given conductivity profile and for different wavelengths. The boundary conditions for the potential are $\Phi_k(z=0\,\mathrm{km})=0$ and $\Phi_k(z=1000\,\mathrm{km})=1$. The vertical profiles for the ionospheric conductivities are taken from the IRI-86 model (BILITZA, 1986) from 80 km at intervals of 1 km up to the altitude of

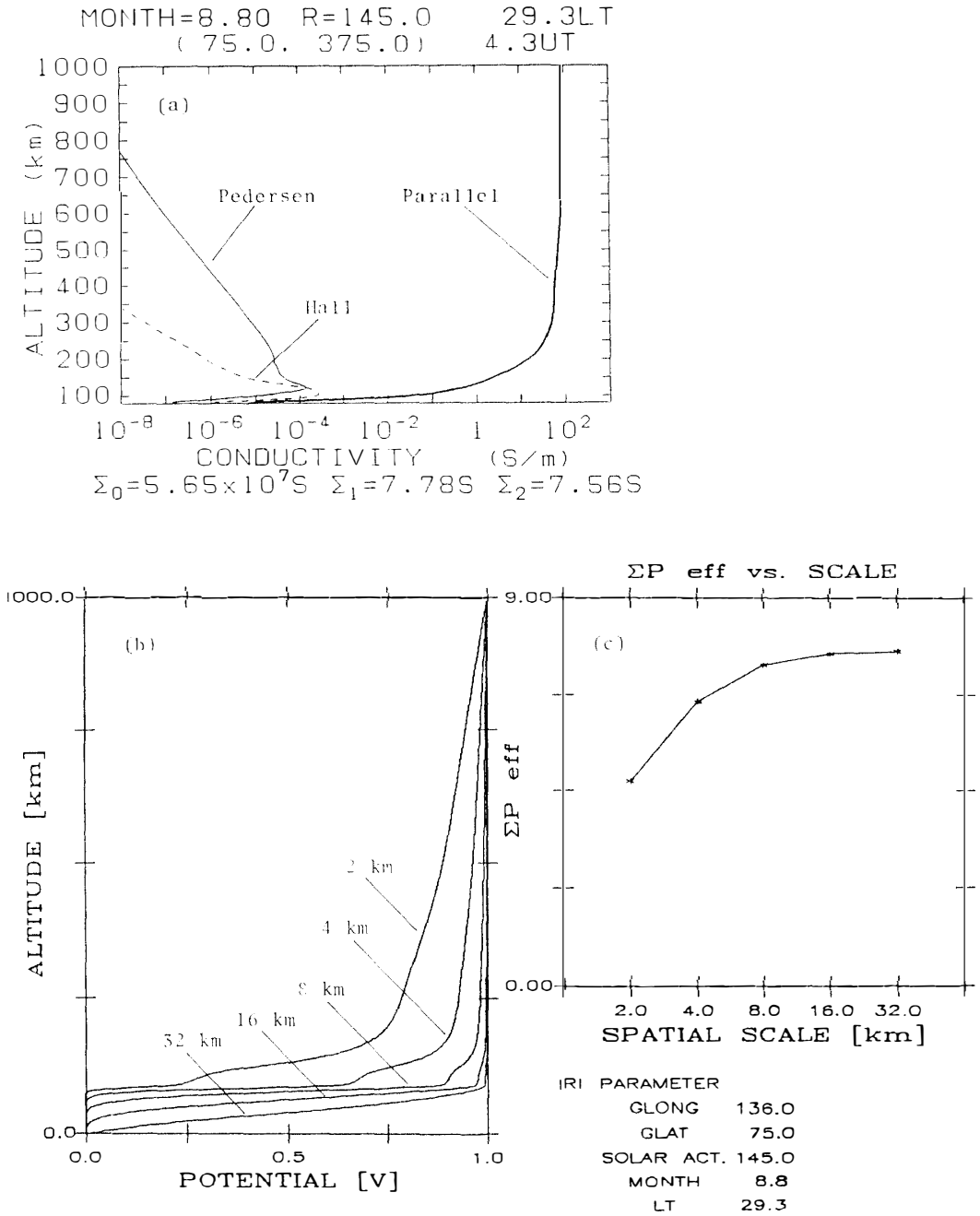

Fig. 1. An example of conductivity profile based on the IRI-86 model and the effective height-integrated Pedersen conductivity $\Sigma_{P,eff}$ calculated from the IRI-86 model. The parameters for the IRI-86 model (season, time, location, and solar activity) are those at the time and location at which the magnetic and electric fields were observed.

a) Conductivity profile of the IRI-86 model. The bold, thin, and dotted lines represent parallel, Pedersen and Hall conductivities.

b) The ionospheric potential profile for each spatial scale-length. It is assumed that $\Phi_k = 1$ at 1000 km and $\Phi_k = 0$ at 0 km altitude.

c) The scale-length dependence of the effective height-integrated Pedersen conductivity $\Sigma_{P,eff}$ calculated from the potential profile in (b).

1000 km. An example of conductivity profile calculated from the IRI-86 model is shown in Fig. 1. It is assumed that both parallel and Pedersen conductivities at the ground are 10^{-13} mho/m, and that the conductivities between 0 km and 80 km are interpolated linearly on logarithmic scale.

The IRI-86 model has parameters representing season, time, locations and solar activity. For these parameters we use the values at the times of observation. The electric field along the z axis can be calculated from the potential Φ. From the eq. (8) in FORGET *et al.*, *i.e.*,

$$\Sigma_{\mathrm{P,eff}} = \frac{1}{E_x(k,z_0)} \int_0^{z_0} \sigma_{\mathrm{P}}(z) E_x(k,z) \mathrm{d}z, \tag{2}$$

we can obtain $\Sigma_{\mathrm{P,eff}}$ which depends on the wave number k.

2.2. *Observations*

The DE-2 spacecraft was launched on August 3, 1981 into a polar orbit with initial apogee and perigee at 1003 km and 299 km altitude, respectively. Vector magnetic field data were obtained by a triaxial fluxgate magnetometer, with resolution of ± 1.5 nT and with a sampling rate of 16 vector samples per second (FARTHING *et al.*, 1981). Vector electric field measurements were made by a symmetric double floating probe system with a sensitivity 0.1 mVm^{-1} and a range ± 1 Vm^{-1} (MAYNARD *et al.*, 1981). One of the horizontal antennas (*i.e.*, along the Z-axis) did not deploy after launch. Data for the electric field along the X-axis and for the magnetic field along the Z-axis are used, where the X-axis is along the spacecraft velocity vector and therefore approximately in the north-south direction; and where the Z-axis is in east-west direction. The $V \times B$ electric field from the satellite motion, the corotation electric field and the contract potential difference are subtracted from the observed electric field. Figure 2 presents an example of the magnetic and electric field perturbations.

The earth's internal magnetic field calculated from a MAGSAT model (LANGEL *et al.*, 1980) is subtracted from the observed magnetic field.

The dayside ionospheric conductivity is primarily determined by the solar EUV and X ray radiation, while the nightside ionospheric conductivity is mainly dependent on auroral particle precipitation. However, the IRI-86 model does not take the effect of particle precipitation into consideration, and therefore we cannot compare the results calculated from the nightside the IRI-86 model directly with those from observations. However, it is of interest to see how much difference there is between the observational results and the calculation based on the nightside the IRI-86 model. Thus one nightside pass (pass 19) is examined for this purpose.

Figure 3 presents the satellite orbits from which data are used. The coordinates in this figure are invariant latitude and invariant magnetic local time. Pass 17 may appear to be a night pass. However, this pass took place near the summer solstice and the terminator at the time of this pass is at a more anti-sunward location than the selected portion of this pass; that is, pass 17 is a sunlit pass. The time of pass 12 is March 13, and this pass crossed the terminator. All other passes are sunlit passes.

Figure 4 shows twenty examples of the scale-length dependence of the ratio $\Delta B_z/\mu_0 E_x$. Digital filters with variable cut-off periods or pass-band periods are used to

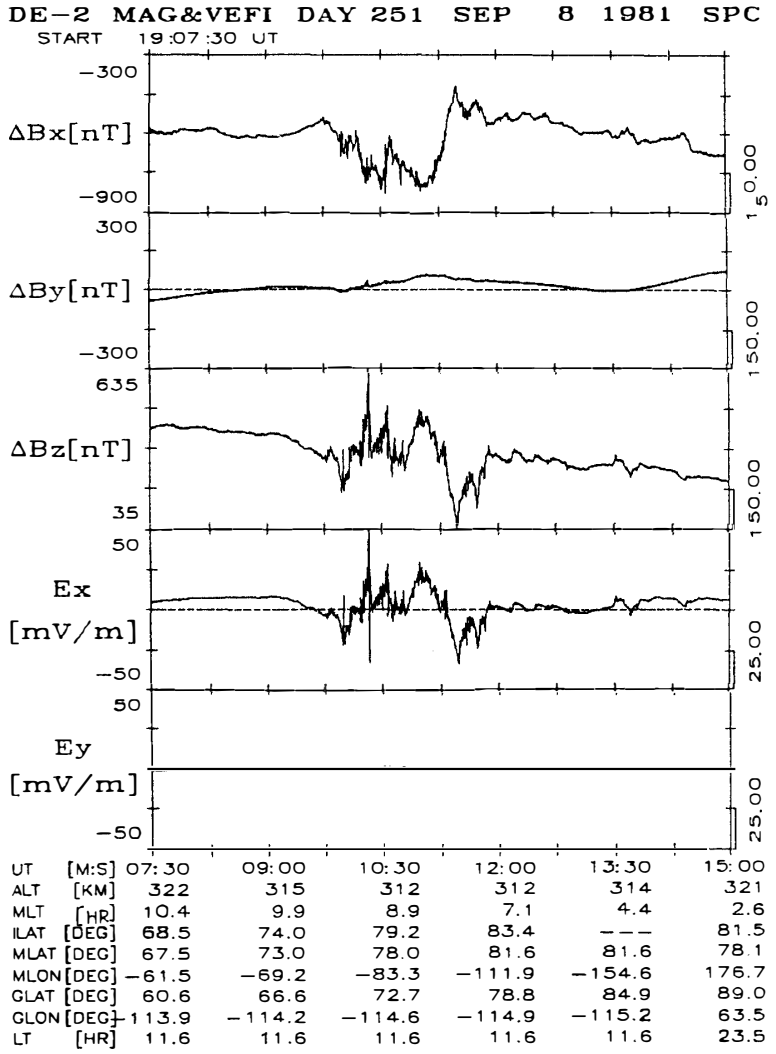

Fig. 2. An example of the magnetic and electric field data observed by DE-2. X-component is along the spacecraft velocity vector, and is approximately in the geographical north-south direction. Y-component is along the vertical, and Z-component is approximately in the east-west direction.

examine the scale-length dependence of the ratio $\Delta B_z/E_x$. The filters used are non-recursive type digital filters, whose transfer functions have insignificant side lobe effects near the cut-off frequencies.

It should be noted that unless the correlation coefficient between the magnetic and electric fields is high, the interpretation of the ratio, $\Delta B_z/E_x$, is not straightforward. The correlation is generally high with data obtained in the sunlit hemisphere. In Fig. 4, only those periods for which the correlation coefficient is higher than 0.5 are connected, and connected lines are omitted for the portions of periods with less correlation.

We investigate the phase difference between the magnetic and electric field perturbations in higher frequencies (using high pass filters whose cut-off period are 2.0 s and 1.0 s). If these perturbations are Alfvén waves, they may have some phase differences each other because of interference between the incident and reflected waves against

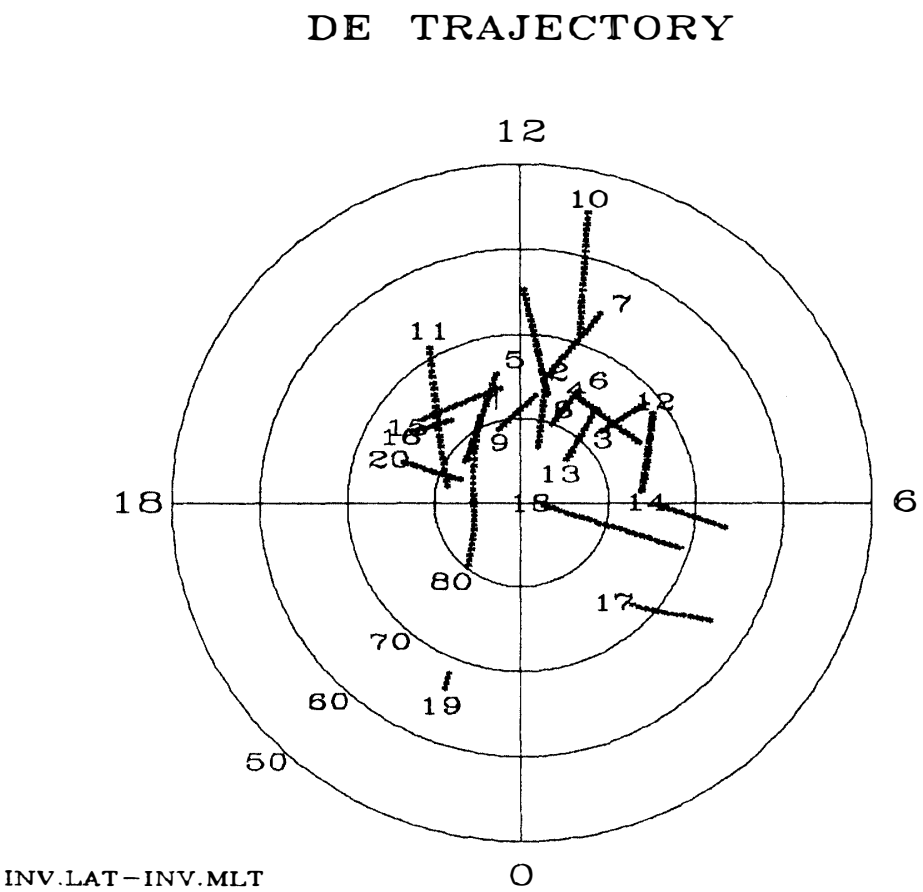

Fig. 3. The plots of 20 satellite passes use. Coordinates are invariant latitude and invariant MLT. Pass 19 is in darkness period, and pass 12 crosses the terminator. Other passes are sunlit passes.

ionosphere. In this case, poor correlation is found between the magnetic and electric field perturbations even if they have similar profiles each other.

Result from the cross correlation between the magnetic and the electric field perturbations shows that 18 in 20 cases have no significant time lags between the magnetic and electric field perturbations. Some parts of data period of case 8 and 15 have a little time lags ($\sim$0.1875 s), but in total region, this time lags do not make any influence with this analysis.

The case labeled 12 in Fig. 4 was observed near the terminator, and the case labeled 19 was observed in the nightside hemisphere.

We assume a power law for the magnetic and electric field power spectral densities. Then, given a frequency band (say, for a band pass filter) the wave energy density is largest at the lower limit of the frequency range. In comparing the observational results on the ratio $\Delta B_z/\mu_0 E_x$ (in a frequency band) with the theoretical results (for a fixed frequency) we assume that the ratio at the frequency of maximum wave energy density in the observation (*i.e.*, at the lower frequency limit of the band pass filter) characterizes the ratio for the frequency band, and we compare this observational ratio with the height-integrated effective Pedersen conductivity, $\Sigma_{P,eff}$, calculated with the IRI-86

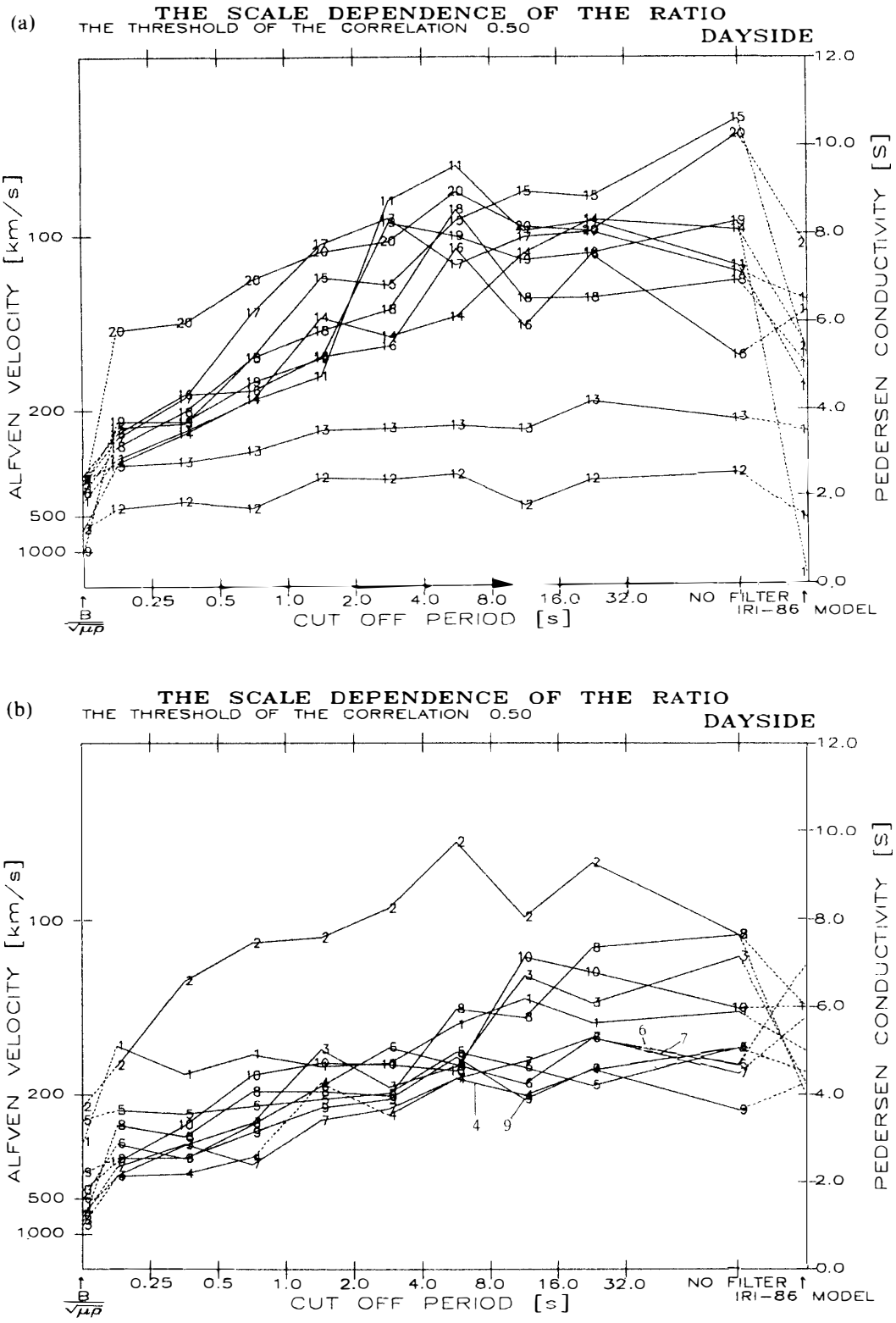

Fig. 4. The scale-length dependence of the ratio $\Delta B_z/\mu_0 E_x$, Alfvén velocity, and Pedersen conductivity for the 20 cases. Pass 12 was observed near the terminator. Pass 19 was observed in darkness. The abscissa represents cut-off periods of high-pass/band-pass filters. The number on each curve corresponds to that in Fig. 3.

model for the same frequency.

3. Results

Figure 5 shows the scale-length dependence of the difference between the effective height-integrated Pedersen conductivity $\Sigma_{P,eff}$ derived from the IRI-86 model and the ratio of ΔB_z to $\mu_0 E_x$ observed by DE-2. The coordinate axis represents this difference.

We use a high-pass or band-pass filter in order to investigate the scale-length dependence of the difference between the model and observation. Since a band-pass filter has cut-off frequencies at both ends, the difference $\Delta B_z/\mu_0 E_x - \Sigma_{P,eff}$ is plotted at the center of each band. The pass numbers marked an each curve correspond to those in Figs. 3 and 4. For each pass (*i.e.*, for each curve in Fig. 5) the difference between the ratio, $\Delta B_z/\mu_0 E_x$, and the Alfvén conductivity $\Sigma_A(=1/(\mu_0 V_A))$ is calculated from the observed plasma density and magnetic field data (assuming that O^+ ions dominate). This difference is plotted at the extreme left on the vertical axis and connected by a dotted line to the rest of the data for the pass. Points for which the correlation between the magnetic and electric field perturbations is poor are connected by dotted lines (*e.g.*, for the large scale-length portion of curve 4).

Many of the curves in Fig. 5 are flat for all scale lengths. But some curves (*e.g.*, curves 6 and 20) show a significant increase with decreasing scale length towards the shortest scale length. Curve 11 has a minimum at a middle scale length (*i.e.*, at the pass band 0.5–1.0 s). For this pass the difference between the maximum and the minimum of $\Delta B_z/\mu_0 E_x - \Sigma_{P,eff}$ is about 4.0 S.

Curve 19 has a different character because this pass is entirely in darkness. The observational ratios are much larger than the theoretical values for this pass. The difference increases with increasing spatial/temporal scale length, and goes off scale at 2–4 s.

In many cases in Fig. 5, the values of $\Delta B_z/\mu_0 E_x - \Sigma_A$ are greater than the values of $\Delta B_z/\mu_0 E_x - \Sigma_{P,eff}$ at the smallest scale length plotted, or what amounts to the same thing, the values of Σ_A are less than the values of $\Delta B_z/\mu_0 E_x$ at the smallest scale length in Fig. 4. Figure 6 shows the scale-length dependence of this relative difference. The format of Fig. 6 is similar to that of Fig. 5 except that the ordinate is a normalized dimensionless quantity.

Some of the profiles of these curves are different from the corresponding profiles in Fig. 5. Curve 19 has a constant value of approximately 1.0. Many of the other curves of others are confined to the level of about ± 0.5. However, parts of curves 6, 7 and 12 are below -0.5. In these cases the ratio $\Delta B_z/\mu_0 E_x$ becomes less than one half of $\Sigma_{P,eff}$ calculated from the IRI-86 model.

We investigated the relation between the *AE* index and the scale-length dependence of the difference $\Delta B_z/\mu_0 E_x - \Sigma_{P,eff}$. However, no clear relationships have thus far been found.

4. Discussions

In Fig. 5 we showed the scale-length dependence of the difference between the ratio

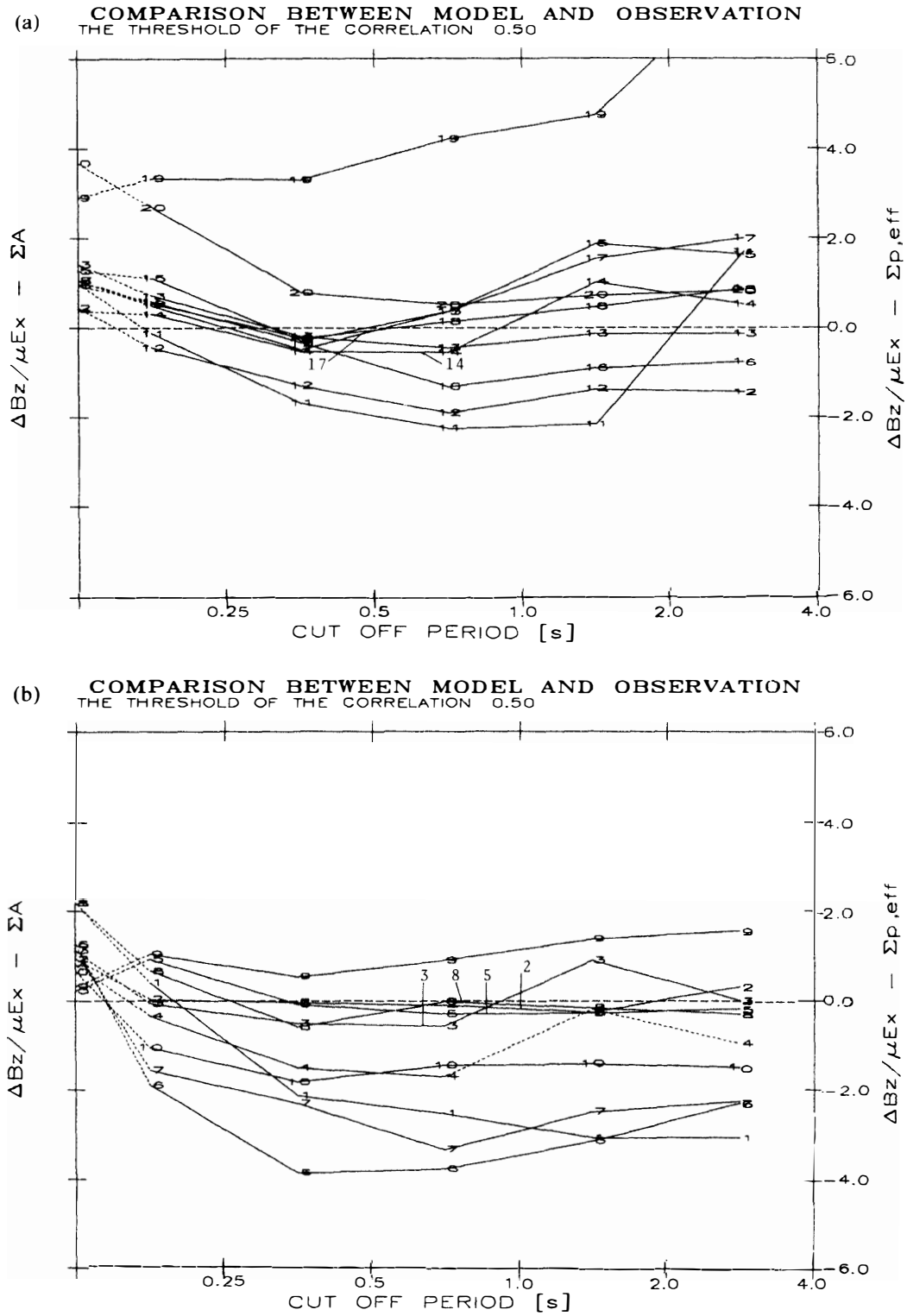

Fig. 5. The scale-length dependence of the difference between the ratio $\Delta B_z/\mu_0 E_x$ and the effective Pedersen conductivity $\Sigma_{P,eff}$.

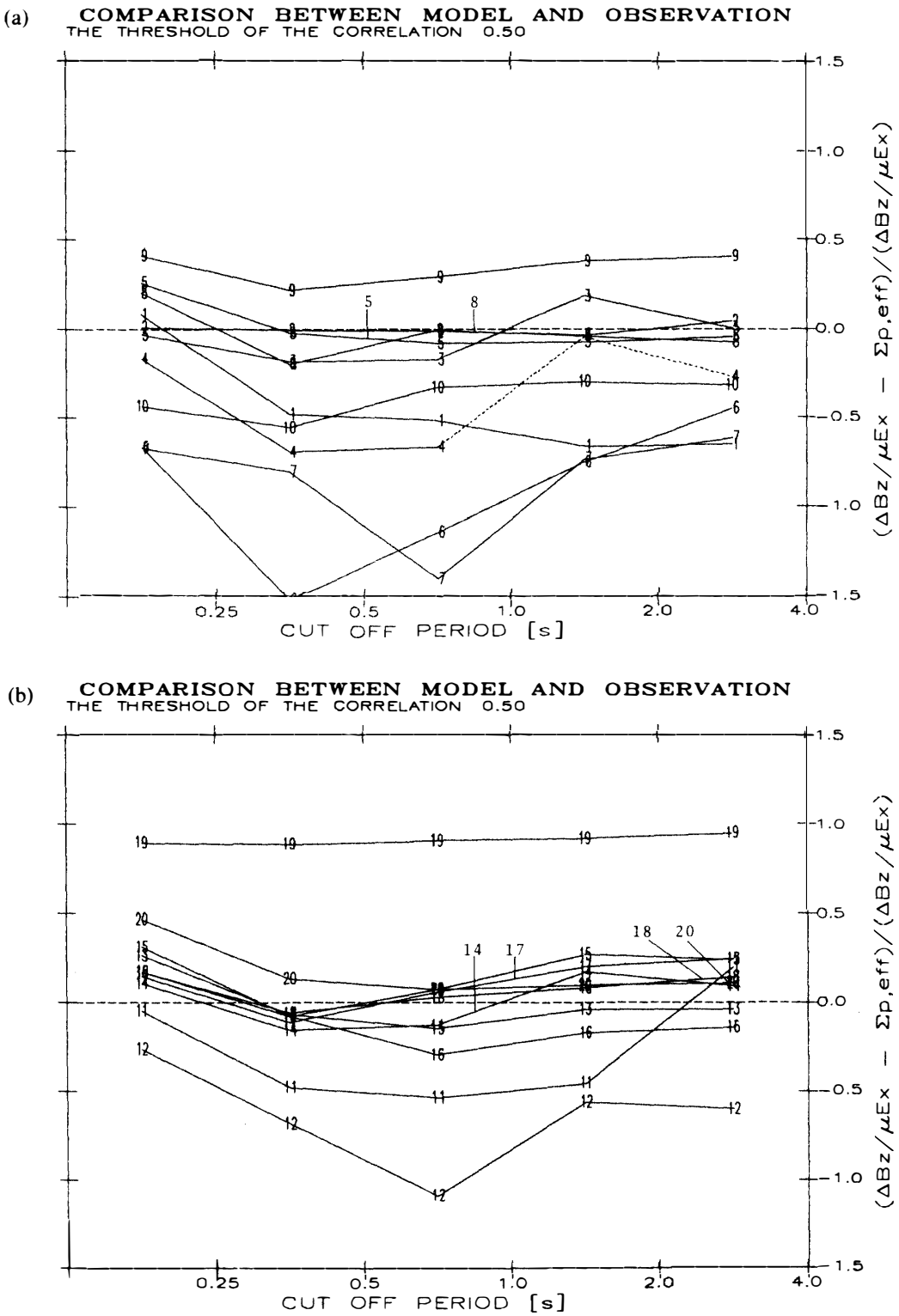

Fig. 6. The scale-length dependence of the normalized difference between the ratio $\Delta B_z/\mu_0 E_x$ and the effective Pedersen conductivity $\Sigma_{P,eff}$.

$\Delta B_z/\mu_0 E_x$ calculated from DE-2 observations and $\Sigma_{P,eff}$ calculated from the IRI-86 model using the method of FORGET *et al.* (1991). If the curves in Fig. 5 are all at zero, this means that $\Delta B_z/\mu_0 E_x - \Sigma_{P,eff}$ on each pass is explained by the model of FORGET *et al.* For example, curves 2, 3 and 5 are near zero for all scale lengths and can be explained by the static model. Some of other curves in Fig. 5 remain near some non-zero constant values.

In a few cases there are poor correlations between the magnetic and electric field perturbations. We interpreted this result with two possibilities. One is a significant variation of ionospheric Pedersen conductivity in small regions, and the other is an existence of localized Alfvén waves in static structures. In the former case, the ratio, $\Delta B_z/E_x$, significantly change in the region where we calculate the correlations. In the latter case, the value of the ratio, $\Delta B_z/E_x$, is not fixed because Σ_A is quite different from Σ_P in many cases on the dayside. In both cases, the correlation between the magnetic and electric field perturbations becomes poor.

Curve 19 has a quite different profile from the others. The reason for this is as follows: There are two main origins in the ionization of the ionosphere; these are solar EUV and X radiation and auroral particle precipitation. On the nightside, the auroral particle precipitation effect becomes dominant. However, the IRI-86 model takes only the solar radiation effect into consideration. Therefore, the calculated $\Sigma_{P,eff}$ from the model gives an underestimate.

In Fig. 6, curve 19 keeps its level near 1.0 through all scale-lengths. Because $\Sigma_{P,eff}$ is much smaller than $\Delta B_z/\mu_0 E_x$ for this case, the ratio $(\Delta B_z/\mu_0 E_x - \Sigma_{P,eff})/(\Delta B_z/\mu_0 E_x)$ is nearly 1.0. For some other passes the difference between the ratio $\Delta B_z/\mu_0 E_x$ and $\Sigma_{P,eff}$ has a scale-length dependence. We can think of two reasons for this behavior. One is the influence of auroral particle precipitation, as in curve 19, and the other is the existence of Alfvén waves. In the former case, the ratio $\Delta B_z/\mu_0 E_x$ increases by auroral particle precipitation because the ionospheric conductivity increases. In the latter case, the existence of Alfvén waves reduces the ratio, $\Delta B_z/\mu_0 E_x$, because Alfvén conductivity Σ_A is generally lower than Σ_P.

In many cases which show scale-length dependence, the minimum is between 0.25 and 1.0 s in the cut off period, and Σ_A is less than $\Delta B_z/\mu_0 E_x$. It appears reasonable to interpret that these minimums reflect the effect of Alfvén waves, because the value, $\Sigma_{P,eff}$ is decreased to $\Delta B_z/\mu_0 E_x$ by Σ_A. We thus speculate that Alfvén waves exist on the temporal scale of 0.25–1.0 s, or, 1–4 Hz. In this respect, there have been reports on the existence of Pc 1–2 magnetic pulsations in the equatorial magnetosphere at $L > 7$ (*e.g.*, ANDERSON *et al.*, 1992).

5. Conclusions

We compared the ratio, $\Delta B_z/\mu_0 E_x$, between the orthogonal magnetic and electric field perturbations in the auroral ionospheric region and the effective Pedersen conductivity calculated with the method of FORGET *et al.* for various scale lengths. Results can be summarized as follows.

1) The differences between the ratio $\Delta B_z/\mu_0 E_x$ from observation and the $\Sigma_{P,eff}$ from model calculation in more than 10 of the 20 cases examined have little dependence on scale length. For these cases, therefore, the scale-length dependence of the ratio

$\Delta B_z/\mu_0 E_x$ can be explained by the model of FORGET *et al.*

2) Several cases show a minimum in the difference between $\Delta B_z/\mu_0 E_x$ and $\Sigma_{P,eff}$ at 0.25–1.0 s. We believe that the primary cause for this scale-length dependence is the presence of Alfvén waves.

Acknowledgments

We wish to thank N. C. MAYNARD for permitting us to use his electric field data in this paper and for his comments. We also wish to thank T. ARAKI, T. TERASAWA, M. TAKEDA, T. KAMEI and S. TAGUCHI for their valuable discussions. This study was supported in part by grant No. 60420013 under the Monbusho Scientific Research Program and by grants No. 63044070 and No. 0330044128 under the Monbusho International Scientific Research Program, the Ministry of Education, Science and Culture, Japan.

References

ANDERSON, B. J., ERLANDSOM, R. E. and ZANETTI, L. J. (1992): A statistical study of Pc 1–2 magnetic pulsations in the equatorial magnetosphere 1. Equatorial occurrence distributions. J. Geophys. Res., **97**, 3075–3088.

BERTHELIER, A., CERISIER, J.-C., BERTHELIER, J.-J., BOSQUED, J.-M. and KOVRAZKHIN, R. A. (1989): The electrodynamic signature of short scale field aligned currents, and associated turbulence in the cusp and dayside auroral zone. Electromagnetic Coupling in the Polar Clefts and Caps, ed. by P. E. SANDHOLT and A. EGELAND. Dordrecht, Kluwer Academic, 299–310.

BILITZA, D. (1986): International reference ionosphere: Recent developments. Radio Sci., **21**, 343–346.

BLOCK, L. P., FALTHAMMAR, C.-G., LINDQVIST, P.-A., MARKLUND, G., MOZER, F. S., PEDERSEN, A., POTEMRA, T. A. and ZANETTI, L. J. (1987): Electric field measurements on VIKING: first results. Geophys. Res. Lett., **14**, 435–438.

DUBININ, E. M., ISRAELEVICH, J.-C. and NIKOLAEVA, N. S. (1990): Auroral electromagnetic disturbances at an altitude of 900 km: The relationship between the electric and magnetic field variations. Planet. Space Sci., **38**, 97–108.

FARTHING, W. H., SUGIURA, M., LEDLEY, B. G. and CAHILL, L. J., JR. (1981): Magnetic field observations on DE-A and -B. Space Sci. Inst., **5**, 551–560.

FORGET, B., CERISIER, J.-C., BERTHELIER, A. and BERTHELIER, J.-J. (1991): Ionospheric closure of small-scale Birkeland currents. J. Geophys. Res., **96**, 1843–1847.

GURNETT, D. A., HUFF, R. L., MENIETTI, J. D., BURCH, J. L., WINNINGHAM, J. D. and SHAWHAN, S. D. (1984): Correlated low-frequency electric and magnetic noise along the auroral field lines. J. Geophys. Res., **89**, 8971–8985.

ISHII, M., SUGIURA, M., IYEMORI, T. and SLAVIN, J. A. (1992): Correlation between magnetic and electric fields in the field-aligned current regions deduced from DE-2 observations. J. Geophys. Res., **97**, 13877–13887.

ISRAELEVICH, P. L., PODGORNY, I. M., KUZMIN, A. K., NIKOLAEVA, N. S. and DUBININ, E. M. (1988): Convection and field-aligned currents, related to polar cap arcs, during strongly Northward IMF (11 January 1983). Planet. Space Sci., **36**, 1317–1328.

KNUDSEN, D. J., KELLEY, M. C., EARLE, G. D., VICKREY, J. F. and BOEHM, M. (1990): Distinguishing Alfvén waves from quasi-static field structures associated with the discrete aurora: Sounding rocket and HILAT satellite measurements. Geophys. Res. Lett., **17**, 921–924.

LANGEL, R. A., ESTES, R. H., MEAD, G. D., FABIANO, E. B. and LANCASTER, E. R. (1980): Initial Geomagnetic Field Model from MAGSAT vector data. Geophys. Res. Lett., **7**, 793–796.

MATSUOKA, A., MUKAI, T., HAYAKAWA, H., KOHNO, Y.-I., TSURUDA, K., NISHIDA, A., OKADA, T.,

KAYA, N. and FUKUNISHI, H. (1991): EXOS-D observations of electric field fluctuations and charged particle precipitation in the polar cusp. Geophys. Res. Lett., **18**, 305–308.

MAYNARD, N. C., BIELECKI, E. A. and BURDICK, H. F. (1981): Instrumentation for vector electric field measurements from DE-B. Space Sci. Inst., **5**, 523–534.

SUGIURA, M. (1984): A fundamental magnetosphere-ionosphere coupling mode involving field-aligned currents as deduced from DE-2 observations. Geophys. Res. Lett., **1**, 877–880.

SUGIURA, M., MAYNARD, N. C., FARTHING, W. H., HEPPNER, J. P., LEDLEY, B. G. and CAHILL, L. J., JR. (1982): Initial results on the correlation between the magnetic and electric fields observed from the DE-2 satellite in the field-aligned current regions. Geophys. Res. Lett., **9**, 985–988.

SUGIURA, M., IYEMORI, T., HOFFMAN, R. A. and MAYNARD, N. C. (1983): Relationships between field-aligned currents, electric fields, and particle precipitation as observed by Dynamics Explorer-2. Magnetospheric Currents, ed. by T. A. POTEMRA. Washington, D.C., Am. Geophys. Union, 96–103 (Geophysical Monograph 28).

WEIMER, D. R., GOERTZ, C. K., GURNETT, D. A., MAYNARD, N. C. and BURCH, J. L. (1985): Auroral zone electric field from DE-1 and 2 at magnetic conjunctions. J. Geophys. Res., **90**, 7479–7494.

WEIMER, D. R., GURNETT, D. A., GOERTZ, C. K., ZANETTI, J. D., BURCH, J. L. and SUGIURA, M. (1987): The current-voltage relationship in auroral current sheets. J. Geophys. Res., **92**, 187–194.

(Received June 23, 1992; Revised manuscript received September 22, 1992)